Aerosols from Overseas Rival Domestic Emissions over North America

Hongbin Yu *et al.*

Science **337**, 566 (2012);
DOI: 10.1126/science.1217576

mass ratio on discharge and charge is $2e^-/O_2$, confirming that the reaction is overwhelmingly Li_2O_2 formation/decomposition. We have also shown that such electrodes are particularly effective at promoting the decomposition of Li_2O_2, with all the Li_2O_2 being decomposed below 4 V and ~50% decomposed below 3.3 V, at a rate approximately one order of magnitude higher than on carbon. Although DMSO is not stable with bare Li anodes, it could be used with protected Li anodes. Nanoporous Au electrodes are not suitable for practical cells, but if the same benefits could be obtained with Au-coated carbon, then low-mass electrodes would be obtained, although cost may still be a problem. A cathode reaction overwhelmingly dominated by Li_2O_2 formation on discharge, its complete oxidation on charge and sustainable on cycling, is an essential prerequisite for a rechargeable nonaqueous Li-O_2 battery. Hence, the results presented here encourage further study of the rechargeable nonaqueous Li-O_2 cell, although many challenges to practical devices remain.

References and Notes

1. K. M. Abraham, Z. Jiang, *J. Electrochem. Soc.* **143**, 1 (1996).
2. P. G. Bruce, S. A. Freunberger, L. J. Hardwick, J.-M. Tarascon, *Nat. Mater.* **11**, 19 (2012).
3. G. Girishkumar, B. McCloskey, A. C. Luntz, S. Swanson, W. Wilcke, *J. Phys. Chem. Lett.* **1**, 2193 (2010).
4. B. Scrosati, J. Hassoun, Y.-K. Sun, *Energy Environ. Sci.* **4**, 3287 (2011).
5. J.-G. Zhang, P. G. Bruce, X. G. Zhang, in *Handbook of Battery Materials*, C. Daniel, J. O. Besenhard, Eds. (Wiley-VCH, Weinheim, Germany, ed. 2, 2011), pp. 759–811.
6. J. Christensen *et al.*, *J. Electrochem. Soc.* **159**, R1 (2012).
7. S. A. Freunberger *et al.*, *J. Am. Chem. Soc.* **133**, 8040 (2011).
8. F. Mizuno, S. Nakanishi, Y. Kotani, S. Yokoishi, H. Iba, *Electrochemistry* **78**, 403 (2010).
9. W. Xu *et al.*, *J. Power Sources* **196**, 3894 (2011).
10. G. M. Veith, N. J. Dudney, J. Howe, J. Nanda, *J. Phys. Chem. C* **115**, 14325 (2011).
11. B. D. McCloskey, D. S. Bethune, R. M. Shelby, G. Girishkumar, A. C. Luntz, *J. Phys. Chem. Lett.* **2**, 1161 (2011).
12. S. A. Freunberger *et al.*, *Angew. Chem. Int. Ed.* **50**, 8609 (2011).
13. H. Wang, K. Xie, *Electrochim. Acta* **64**, 29 (2012).
14. H.-G. Jung, J. Hassoun, J.-B. Park, Y.-K. Sun, B. Scrosati, *Nat. Chem.* **4**, 579 (2012).
15. Materials and methods are available as supplementary materials on *Science* Online.
16. C. O. Laoire, S. Mukerjee, K. M. Abraham, E. J. Plichta, M. A. Hendrickson, *J. Phys. Chem. C* **114**, 9178 (2010).
17. Z. Peng *et al.*, *Angew. Chem. Int. Ed.* **50**, 6351 (2011).
18. B. D. McCloskey *et al.*, *J. Phys. Chem. Lett.* **3**, 997 (2012).
19. A. Débart, A. J. Paterson, J. Bao, P. G. Bruce, *Angew. Chem. Int. Ed.* **47**, 4521 (2008).
20. C. J. Allen, S. Mukerjee, E. J. Plichta, M. A. Hendrickson, K. M. Abraham, *J. Phys. Chem. Lett.* **2**, 2420 (2011).
21. Y.-C. Lu *et al.*, *Energy Environ. Sci.* **4**, 2999 (2011).
22. Y.-C. Lu, H. A. Gasteiger, Y. Shao-Horn, *J. Am. Chem. Soc.* **133**, 19048 (2011).
23. T. Ogasawara, A. Débart, M. Holzapfel, P. Novák, P. G. Bruce, *J. Am. Chem. Soc.* **128**, 1390 (2006).
24. B. D. McCloskey *et al.*, *J. Am. Chem. Soc.* **133**, 18038 (2011).
25. S. J. Visco, B. D. Katz, Y. S. Nimon, L. D. DeJonghe, U.S. Patent 7,282,295 (2007).
26. X.-H. Yang, P. He, Y.-Y. Xia, *Electrochem. Commun.* **11**, 1127 (2009).
27. J. Read, *J. Electrochem. Soc.* **149**, A1190 (2002).
28. Y. G. Wang, H. S. Zhou, *J. Power Sources* **195**, 358 (2010).
29. J. S. Hummelshøj *et al.*, *J. Chem. Phys.* **132**, 071101 (2010).
30. V. S. Bryantsev, M. Blanco, F. Faglioni, *J. Phys. Chem. A* **114**, 8165 (2010).
31. Y. Mo, S. P. Ong, G. Ceder, *Phys. Rev. B* **84**, 205446 (2011).
32. D. Aurbach, M. Daroux, P. Faguy, E. Yeager, *J. Electroanal. Chem.* **297**, 225 (1991).
33. J. Hassoun, F. Croce, M. Armand, B. Scrosati, *Angew. Chem. Int. Ed.* **50**, 2999 (2011).

Acknowledgments: P.G.B. is indebted to the UK Engineering and Physical Sciences Research Council, including the Supergen Programme and Alistore for financial support.

Supplementary Materials

www.sciencemag.org/cgi/content/full/science.1223985/DC1
Materials and Methods
Figs. S1 to S9
References (*34*, *35*)

30 April 2012; accepted 26 June 2012
Published online 19 July 2012;
10.1126/science.1223985

Aerosols from Overseas Rival Domestic Emissions over North America

Hongbin Yu,[1,2]* Lorraine A. Remer,[3] Mian Chin,[2] Huisheng Bian,[2,3] Qian Tan,[2,4] Tianle Yuan,[2,3] Yan Zhang[2,4]

Many types of aerosols have lifetimes long enough for their transcontinental transport, making them potentially important contributors to air quality and climate change in remote locations. We estimate that the mass of aerosols arriving at North American shores from overseas is comparable with the total mass of particulates emitted domestically. Curbing domestic emissions of particulates and precursor gases, therefore, is not sufficient to mitigate aerosol impacts in North America. The imported contribution is dominated by dust leaving Asia, not by combustion-generated particles. Thus, even a reduction of industrial emissions of the emerging economies of Asia could be overwhelmed by an increase of dust emissions due to changes in meteorological conditions and potential desertification.

Atmospheric aerosols emitted or produced in one region can be transported thousands of miles downwind to affect other regions on intercontinental or hemispheric scales (*1*–*3*). Because of such intercontinental transport, emission controls over North America may be offset partly by the import of aerosols from remote international sources. Assessing the aerosol intercontinental transport and its impacts on atmospheric composition, air quality, and climate in North America is thus needed from both scientific and policy perspectives. Currently, such assessment for the most part has been based on global model simulations (*4*–*6*) and remains very uncertain (*7*).

Today's constellation of passive and active satellite sensors are providing three-dimensional distributions of aerosol properties on a global scale, with improved accuracy for aerosol optical depth (AOD) and enhanced capability of characterizing aerosol type (*8*). Such advances have made it feasible to elucidate the evolution of aerosol plumes during the cross-ocean transport (*9*, *10*) and generate measurement-based estimates of aerosol intercontinental transport on seasonal and annual time scales (*11*, *12*).

We integrated satellite measurements from the Moderate-resolution Imaging Spectroradiometer (MODIS) (*13*) and the Cloud-Aerosol Lidar with Orthogonal Polarization (CALIOP) (*14*) in order to characterize the three-dimensional distributions of trans-Pacific dust transport (*15*). We used MODIS measurements of total AOD and fine-mode fraction over ocean to separate AOD for dust, combustion aerosol, and marine aerosol (*16*). Combustion aerosol refers to aerosol products from the burning of both biomass and fossil fuels, which include sulfates, nitrates, and carbonaceous particles. The partitioning of AOD into these three categories accounts for fine-mode components of marine and dust aerosol (*15*, *16*). The CALIOP measurements are used to characterize seasonal variations of aerosol extinction profiles, with dust being separated from other types of aerosols by the measured depolarization ratio (*15*). The climatology of springtime (March-April-May, or MAM) AOD (2001–2007) and vertical profile of extinction (2006–2010) over the North Pacific basin are shown in Fig. 1. Spring is the most active season for trans-Pacific transport of combustion aerosols and dust because of the combined effect of active extratropical cyclones and the strongest mid-latitude westerlies. However, trans-Pacific transport occurs throughout the year (*12*). Over the period we examined here, interannual variations of AOD are generally small for dust in the outflow and inflow regions (8 and 4%, respectively), but larger (17 and 18%, respectively) for combustion aerosol. The relatively large interannual variations for combustion

[1]Earth System Science Interdisciplinary Center, University of Maryland, College Park, MD 20740, USA. [2]Earth Science Directorate, NASA Goddard Space Flight Center, Greenbelt, MD 20771, USA. [3]Joint Center for Earth Systems Technology, University of Maryland at Baltimore County, Baltimore, MD 21228, USA. [4]Goddard Earth Sciences Technology and Research Center, Universities Space Research Association, Columbia, MD 21044, USA.

*To whom correspondence should be addressed. E-mail: hongbin.yu@nasa.gov

aerosols are likely attributable to the large interannual variations of Eurasian fires, such as the intensive fires in 2003 and 2008 (*17*).

As evident in Fig. 1, elevated dust and combustion AOD stretches more than 10,000 km from East Asian to North American coasts. The CALIOP climatology of vertical profiles in the exported region as shown in Fig. 1 reveal that dust transported to the northwestern Pacific extends in the vertical from the surface to more than 10 km, which is generally consistent with the multilayered structure as documented in previous studies (*18*–*20*). During the trans-Pacific transport, dust in the lower layers is largely removed, whereas dust in the upper layers escapes removal. This results in the elevated dust layers at 2 to 6 km in the northeastern Pacific. For nondust profiles, marine aerosols contribute to the large aerosol extinction in the marine boundary layer.

The dust extinction or AOD in a layer derived from MODIS and CALIOP was converted to mass concentration by using the prescribed mass extinction efficiency for dust based on in situ observations (*21*). The dust mass flux was then calculated by using zonal wind speed from the Goddard Earth Observing System–Data Assimilation System (GEOS-DAS), version 4. The MODIS-CALIOP–integrated (denoted as MODIOP) estimates of dust fluxes for 2005 are shown in Fig. 2A. On an annual basis, 140 Tg (1 Tg = 10^{12} g = 10^{6} tons) of dust is exported from East Asia. After the trans-Pacific transport, 56 Tg of dust reaches the west coast of North America. The remaining 84 Tg is deposited into the North Pacific and/or transported to the Arctic. The CALIOP vertical profiles allow us to estimate dust fluxes in different altitude ranges (fig. S1). The trans-Pacific dust transport occurs predominantly above the boundary layer. Only ~3 Tg or 5.4% of dust enters North America through the lowest 2-km layer, and it is this fraction that may be most relevant to air quality, mainly in the west part of North America.

A satellite perspective of the contribution of foreign sources to the aerosol amount over North America is shown in Fig. 2B, defined as a box 25° to 60°N, 75° to 125°W. The total annual import of aerosols amounts to 64 Tg, including 56 Tg of dust via trans-Pacific transport, 4 Tg of combustion aerosols also via trans-Pacific transport (*12*), and an additional 4 Tg of Saharan dust via trans-Atlantic transport (north of 20°N) (*11*). Clearly, the imported aerosol mass is dominated (88%) by the trans-Pacific transport of dust. The total mass of imported particles is nearly equivalent to the estimated total (69 Tg) of domestic emissions and production of particulate matter in North America (*15*), as defined as particles with diameters less than 10 μm (PM_{10}) and shown in Fig. 2C. The trans-Pacific dust has not only Asian (49 to 77%, depending on season) but also African (15 to 34%) and Middle Eastern (7 to 17%) origins (fig. S2), as shown by the Goddard Chemistry Aerosol Radiation and Transport (GOCART) and the Global Modeling Initiative (GMI) model simulations (*15*). Similarly, the trans-Pacific pollution originates from not only East Asia (54 to 72%) but also Europe (22 to 34%) and South Asia (5 to 13%) (fig. S2).

It is difficult to quantify the uncertainties associated with these measurement-based estimates of aerosol mass flux. Previous work (*12*) suggests that uncertainties of the absolute magnitude of the mass flux estimated in similar manner are on an order of a factor of 2, with major uncertainty introduced from uncertainty in retrieved AOD and aerosol transport height. In this study, two improvements have been made that should reduce uncertainties. First, aerosol transport heights are better known because of the multiyear CALIOP data, whereas previously aerosol transport heights were largely assumed on the basis of very limited measurements. Second, the AOD product has been corrected for cloud contamination. We anticipate that the uncertainty has been reduced, but it remains challenging to quantify. If we assume that the CALIOP measurements of vertical profile shape are perfect and cloud contamination correction reduces AOD uncertainty by 20%, a ballpark estimate that bounds mass flux uncertainty would be 55 to 100%. Even if these improvements do not reduce uncertainty of the absolute magnitude of the estimates, consistency of the method allows for the identification of seasonal variations, meridional distributions, and relative differences between export and import locations or transport efficiency.

The satellite-based estimates of trans-Pacific dust mass flux differ from those computed by the GOCART (*22*) and the GMI (*23*) models, with major differences occurring in seasonal variations and meridional distributions, as shown in Fig. 3. The annual dust flux exported from East Asia is estimated to be about 133 and 122 Tg from GOCART and GMI, respectively, which is 5 to 13% lower than the satellite estimate. The dust flux inflow to North America is calculated to be 45 and 30 Tg by GOCART and GMI, respectively, which represents an underestimate of 18 and 46% as compared with the satellite-based estimate. The lower transport efficiency by GMI results is presumably from more efficient dust scavenging by convection in the GMI model than in GOCART.

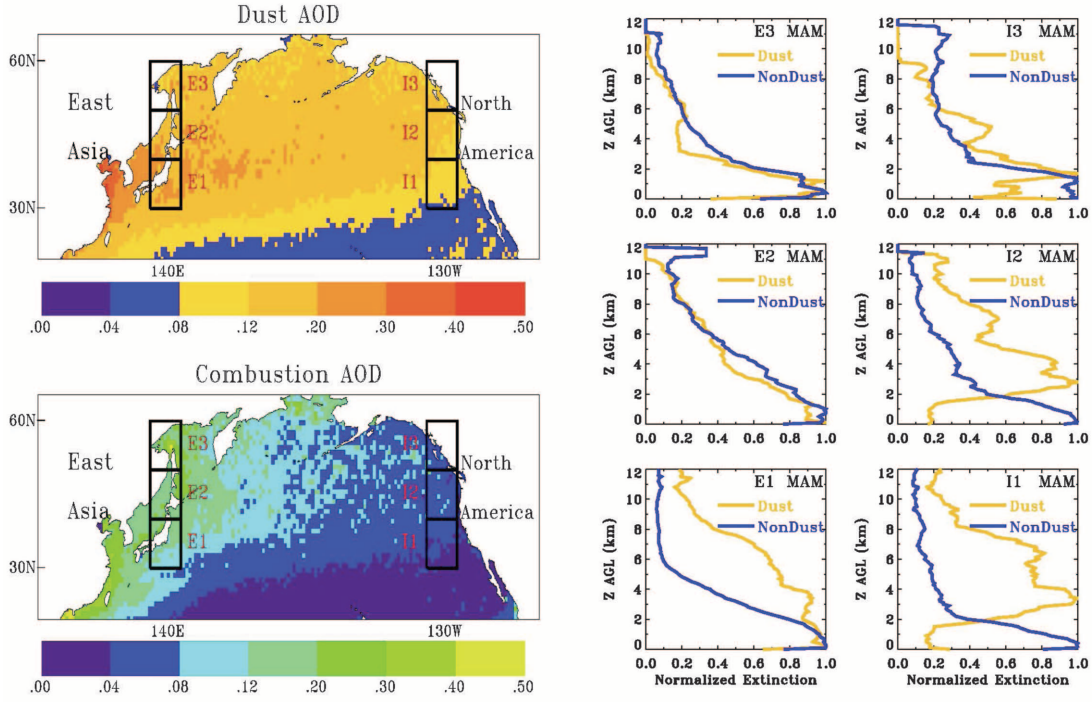

Fig. 1. A satellite-based climatology of springtime (March-April-May, or MAM) trans-Pacific transport of aerosols. (**Left**) Columnar AOD over the North Pacific for dust and combustion aerosols derived from 2001–2007 MODIS measurements. (**Right**) Normalized extinction profiles (with respect to corresponding maximum extinction) for dust and nondust (including combustion and marine origin) aerosols, derived from 2006–2010 CALIOP measurements, over three export regions (E1, E2, and E3) and three import regions (I1, I2, and I3) as defined at left.

To demonstrate the impact of these imported particles on North American regional climate, we estimated the direct radiative effect (DRE) over North America contributed by the imports (*15*). To do so, we had to characterize the evolution of the imported aerosol amount over the continent itself rather than the ocean, and we did this by using GOCART and GMI results of source-receptor relationship experiments (*15*). Aerosol optical properties were characterized according to the Aerosol Robotic Network (AERONET) measurements (*24*). Collectively, the imported pollution and dust introduces a reduction of cloud-free net solar radiation of –1.7 [–1.5, –1.9] and –3.0 [–2.6, –3.4] Wm^{-2} at top-of-atmosphere (TOA) and surface, respectively, which represents 31% (24 to 40%) and 37% (28 to 48%) of the total DRE over North America (Fig. 4). In spring, the imported aerosols make the greatest contribution to the DRE (fig. S5). DRE by the imported pollution accounts for as much as 31 to 59% of that by the imported dust, although the imported dust mass is an order of magnitude larger than the imported pollution aerosol mass. This is because the combustion aerosols scatter and absorb the solar radiation in a more effective way than does dust. Besides the aerosol DREs discussed above, the imported aerosols could exert substantial effects in many other ways, such as changing atmospheric stability by absorbing solar radiation (*25*, *26*), altering cloud and precipitation processes through acting as ice nuclei (*27*), and accelerating the melting of snow in the Sierra Nevada by deposition on snow (*28*).

In comparison, the imported aerosols would have less substantial impacts on air quality of North America. Although the domestic emissions are all near the surface, the imported aerosols are predominantly above the boundary layer, as previously noted. So dust may substantially affect near-surface aerosol concentrations only in parts of the western United States and Canada and on an episodic basis. In other regions, curbing domestic emissions should still be the most efficient way for controlling air pollution (*5*). This differs from imported ozone, which has longer lifetime than aerosols and can continuously form via photochemistry during oceanic transport.

Because of the long-range transport, dust makes a substantial contribution to AOD away from strong anthropogenic sources, as noted in Fig. 1. Interpretation of AOD for a variety of applications, including aerosol-cloud interaction, should consider the possibility of a substantial portion of dust in the mix.

Clearly assessing and mitigating the impacts of imported aerosols requires a modeling system that links the local, regional, intercontinental, and global scales. Satellite measurements as discussed in this study provide an observational benchmark to evaluate and constrain the model simulations. Although this study focuses on the impacts of intercontinental transport into North America, aerosols emitted and produced in North

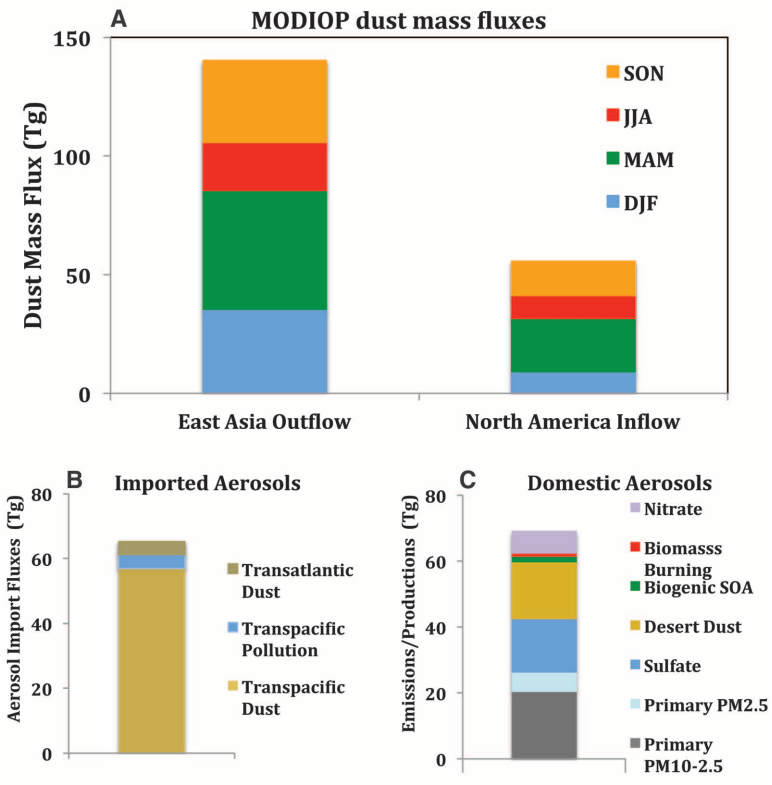

Fig. 2. (**A**) Satellite-based estimate of dust mass flux in East Asia outflow and North America inflow. (**B**) The import of aerosols to North America is 64 Tg/a, including trans-Pacific dust and pollution aerosols and trans-Atlantic dust, is comparable with (**C**) the annual emissions and productions of aerosols of 69 Tg/a from major domestic sources in North America. Primary PM emissions include only anthropogenic sources (excluding prescribed fires).

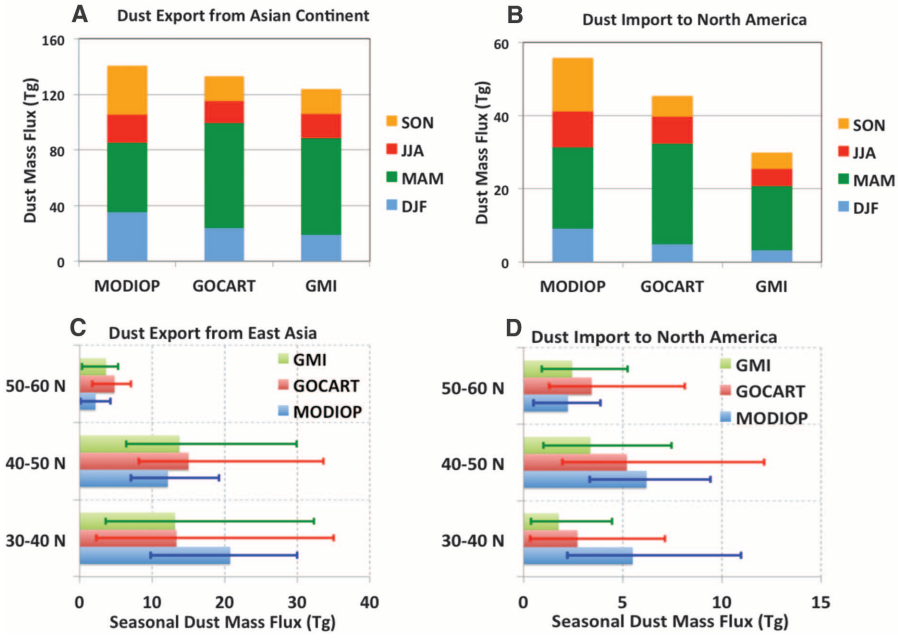

Fig. 3. Comparisons of satellite (MODIOP) and model (GOCART and GMI) estimates of dust export flux from the Asian continent (**A** and **C**) and dust import flux to North America (**B** and **D**). Meridionally integrated dust mass fluxes are shown in (A) and (B) with seasonal distinction, and meridional distributions of seasonal dust mass fluxes are shown in (C) and (D), with boxes and error bars representing mean and range of seasonal mass flux, respectively.

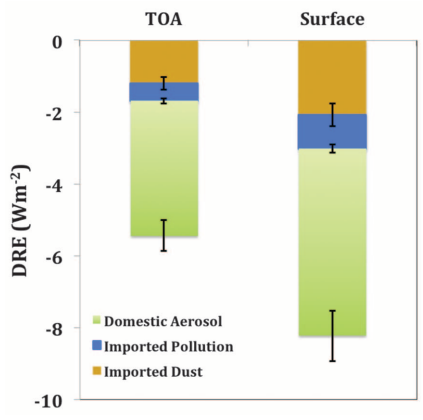

Fig. 4. Estimated clear-sky DRE (watts per square meter) on solar radiation at top-of-atmosphere (TOA) and surface by imported pollution and dust, as well as North American domestic aerosol. Collectively imported dust and pollution aerosols contribute 24 to 41% and 28 to 48% of aerosol-induced total reduction of solar radiation at TOA and surface, respectively. Error bars indicate the range of DRE for perturbing aerosol single-scattering albedo by ±0.03.

America also affect other regions via intercontinental transport. To mitigate aerosol impacts on regional climate change, actions by a single nation are inadequate. The world must work cooperatively and act synchronically to meet the challenges of global health on a changing planet. Focusing on the carbon budget and urban/industrial pollution sources is also inadequate because the imported dust dominates the mass budget and aerosol DREs. Dust emissions can respond to climate changes, such as changes of wind, precipitation, and vegetation. It is thus essential to acquire better understanding of the interactions between dust and climate.

References and Notes

1. J. M. Prospero, E. Blades, G. Mathison, R. Naidu, *Aerobiologia* **21**, 1 (2005).
2. P. E. Biscaye, F. E. Grousset, A. M. Svensson, A. Bory, L. A. Barrie, *Science* **290**, 2258 (2000).
3. R. B. Husar *et al.*, *J. Geophys. Res.* **106**, 18317 (2001).
4. C. L. Heald *et al.*, *J. Geophys. Res.* **111**, D14310 (2006).
5. M. Chin, T. Diehl, P. Ginoux, W. Malm, *Atmos. Chem. Phys.* **7**, 5501 (2007).
6. J. Liu, D. L. Mauzerall, L. W. Horowitz, *Atmos. Chem. Phys.* **8**, 3721 (2008).
7. F. Dentener, T. Keating, H. Akimoto, Eds., *Hemispheric Transport of Air Pollution* (Air Pollution Studies No. 17, United Nations, Geneva, 2010).
8. H. Yu *et al.*, in *Atmospheric Aerosol Properties and Climate Impacts, A Report by the U.S. Climate Change Science Program and the Subcommittee on Global Change Research*, M. Chin, R. A. Kahn, S. E. Schwartz, Eds. (NASA, Washington, DC, 2009).
9. O. V. Kalashnikova, R. A. Kahn, *J. Geophys. Res.* **113**, D24204 (2008).
10. Z. Liu *et al.*, *J. Geophys. Res.* **113**, D07207 (2008).
11. Y. J. Kaufman *et al.*, *J. Geophys. Res.* **110**, D10S12 (2005).
12. H. Yu *et al.*, *J. Geophys. Res.* **113**, D14S12 (2008).
13. L. A. Remer *et al.*, *J. Geophys. Res.* **113**, D14S07 (2008).
14. D. M. Winker *et al.*, *Bull. Am. Meteorol. Soc.* **91**, 1211 (2010).
15. Materials and methods are available as suppplementary materials on *Science* Online.
16. H. Yu *et al.*, *J. Geophys. Res.* **114**, D10206 (2009).
17. C. Warneke *et al.*, *Geophys. Res. Lett.* **36**, L02813 (2009).
18. J. L. Stith *et al.*, *J. Geophys. Res.* **114**, D05207 (2009).
19. A. Zhu, V. Ramanathan, F. Li, D. Kim, *J. Geophys. Res.* **112**, D16208 (2007).
20. L. Su, O. B. Toon, *Atmos. Chem. Phys.* **11**, 3263 (2011).
21. H. Maring, D. L. Savoie, M. A. Izaguirre, L. Custals, J. S. Reid, *J. Geophys. Res.* **108**, 8592 (2003).
22. M. Chin *et al.*, *Ann. Geophys.* **27**, 3439 (2009).
23. H. Bian *et al.*, *Atmos. Chem. Phys.* **9**, 2375 (2009).
24. T. F. Eck *et al.*, *J. Geophys. Res.* **110**, D06202 (2005).
25. V. Ramanathan, G. Carmichael, *Nat. Geosci.* **1**, 221 (2008).
26. H. Yu, S. C. Liu, R. E. Dickinson, *J. Geophys. Res.* **107**, 4142 (2002).
27. K. Sassen, *Geophys. Res. Lett.* **29**, 1465 (2002).
28. O. L. Hadley, C. E. Corrigan, T. W. Kirchstetter, S. Cliff, V. Ramanathan, *Atmos. Chem. Phys.* **10**, 7505 (2010).

Acknowledgments: We acknowledge the NASA support of this work via NNXAH66G (The Science of Terra and Aqua Program) and NNX11AJ91G (Atmospheric Composition Modeling and Analysis Program) (H.Y.), both managed by R. Eckman. The NASA Modeling, Analysis, and Prediction program managed by D. Considine is acknowledged for supporting the model development of GOCART (M.C.) and GMI (H.B., under NNX10AK61G). We are grateful to J. Zhang for providing his reprocessed MODIS data, Z. Liu for providing insights in the lidar characterization of Asian dust, and X. Pan for acquiring CALIOP data. The MODIS data were obtained from the NASA Level 1 and Atmosphere Archive and Distribution System. The CALIOP data were obtained from the NASA Langley Research Center Atmospheric Science Data Center.

Supplementary Materials

www.sciencemag.org/cgi/content/full/337/6094/566/DC1
Materials and Methods
Figs. S1 to S6
References (*29*–*46*)

6 December 2011; accepted 12 June 2012
10.1126/science.1217576

Aerial Photographs Reveal Late–20th-Century Dynamic Ice Loss in Northwestern Greenland

Kurt H. Kjær,[1]* Shfaqat A. Khan,[2] Niels J. Korsgaard,[1] John Wahr,[3] Jonathan L. Bamber,[4] Ruud Hurkmans,[4] Michiel van den Broeke,[5] Lars H. Timm,[1] Kristian K. Kjeldsen,[1] Anders A. Bjørk,[1] Nicolaj K. Larsen,[6] Lars Tyge Jørgensen,[7] Anders Færch-Jensen,[7] Eske Willerslev[1]

Global warming is predicted to have a profound impact on the Greenland Ice Sheet and its contribution to global sea-level rise. Recent mass loss in the northwest of Greenland has been substantial. Using aerial photographs, we produced digital elevation models and extended the time record of recent observed marginal dynamic thinning back to the mid-1980s. We reveal two independent dynamic ice loss events on the northwestern Greenland Ice Sheet margin: from 1985 to 1993 and 2005 to 2010, which were separated by limited mass changes. Our results suggest that the ice mass changes in this sector were primarily caused by short-lived dynamic ice loss events rather than changes in the surface mass balance. This finding challenges predictions about the future response of the Greenland Ice Sheet to increasing global temperatures.

Mass loss from the Greenland Ice Sheet is a complex function of processes related to surface mass balance (SMB) and dynamic ice loss (DIL) that are forced by fluctuations in atmospheric and oceanic energy input (*1*). SMB is the difference between accumulation from solid precipitation (snow) and mass loss from ablation (ice melt and sublimation). DIL is related to marine-terminating outlets due to the marginal breakup of floating ice tongues and to subsequent accelerated flow caused by decreased buttressing and reduced basal drag, resulting in thinning (decreasing ice surface elevations) (*2*–*4*). The relative role of SMB to DIL in contributing to marginal ice mass loss remains contentious (*5*–*7*).

Only limited observational evidence of ice mass changes exists before the 21st century, when space-based observations from interferometric synthetic aperture radar (InSAR), intensity tracking

[1]Centre for GeoGenetics, Natural History Museum, University of Copenhagen, Copenhagen, Denmark. [2]DTU Space–National Space Institute, Technical University of Denmark, Department of Geodesy, Lyngby, Denmark. [3]Department of Physics and Cooperative Institute for Research in Environmental Sciences, University of Colorado, Boulder, CO, USA. [4]Bristol Glaciology Centre, University of Bristol, Bristol, UK. [5]Institute for Marine and Atmospheric Research, Utrecht University, Utrecht, Netherlands. [6]Department of Geoscience, Aarhus University, Aarhus, Denmark. [7]Danish National Cadastre and Survey, Copenhagen, Denmark.

*To whom correspondence should be addressed. E-mail: kurtk@snm.ku.dk